

Article

Dynamic Analysis of the Median Nerve in Carpal Tunnel Syndrome from Ultrasound Images Using the YOLOv5 Object Detection Model

Shuya Tanaka , Atsuyuki Inui * , Yutaka Mifune, Hanako Nishimoto, Issei Shinohara, Takahiro Furukawa, Tatsuo Kato, Masaya Kusunose, Yutaka Ehara, Shunsaku Takigami and Ryosuke Kuroda

Department of Orthopaedic Surgery, Graduate School of Medicine, Kobe University, 5-2, Kusunoki-cho 7, Chuo-ku, Kobe-shi 650-0017, Japan; shuyat@med.kobe-u.ac.jp (S.T.)

* Correspondence: ainui@med.kobe-u.ac.jp; Tel.: +81-78-382-5111; Fax: +81-78-351-6944

Abstract: Carpal tunnel syndrome (CTS) is caused by subsynovial connective tissue fibrosis, resulting in median nerve (MN) mobility. The standard evaluation method is the measurement of the MN cross-sectional area using static images, and dynamic images are not widely used. In recent years, remarkable progress has been made in the field of deep learning (DL) in medical image processing. The aim of the present study was to evaluate MN dynamics in CTS hands using the YOLOv5 model, which is one of the object detection models of DL. We included 20 normal hands (control group) and 20 CTS hands (CTS group). We obtained ultrasonographic short-axis images of the carpal tunnel and the MN and recorded MN motion during finger flexion–extension, and evaluated MN displacement and velocity. The YOLOv5 model showed a score of 0.953 for precision and 0.956 for recall. The radial–ulnar displacement of the MN was 3.56 mm in the control group and 2.04 mm in the CTS group, and the velocity of the MN was 4.22 mm/s in the control group and 3.14 mm/s in the CTS group. The scores were significantly reduced in the CTS group. This study demonstrates the potential of DL-based dynamic MN analysis as a powerful diagnostic tool for CTS.

Keywords: carpal tunnel syndrome; ultrasound; YOLO



Citation: Tanaka, S.; Inui, A.; Mifune, Y.; Nishimoto, H.; Shinohara, I.; Furukawa, T.; Kato, T.; Kusunose, M.; Ehara, Y.; Takigami, S.; et al. Dynamic Analysis of the Median Nerve in Carpal Tunnel Syndrome from Ultrasound Images Using the YOLOv5 Object Detection Model. *Appl. Sci.* **2023**, *13*, 13256. <https://doi.org/10.3390/app132413256>

Academic Editors: Donato Cascio, Chrysostomos Stylios and Voula Georgopoulos

Received: 30 September 2023

Revised: 11 December 2023

Accepted: 13 December 2023

Published: 14 December 2023



Copyright: © 2023 by the authors. Licensee MDPI, Basel, Switzerland. This article is an open access article distributed under the terms and conditions of the Creative Commons Attribution (CC BY) license (<https://creativecommons.org/licenses/by/4.0/>).

1. Introduction

Carpal tunnel syndrome (CTS) is the most common entrapment neuropathy [1], occurring in 3.8% of the general population [2]. The condition manifests within the confines of the carpal tunnel, a narrow space through which the median nerve (MN) and nine flexor tendons pass. These tendons consist of the flexor pollicis longus (FPL), four flexor digitorum superficialis (FDS), and the four flexor digitorum profundus (FDP). Located within the carpal tunnel, these important anatomical structures are enveloped by a multilayered structure known as the subsynovial connective tissue (SSCT) [3,4]. While this SSCT plays an essential role in cushioning and protecting these delicate nerve and tendon structures, it can become a source of concern in CTS patients. The histologic examination of the SSCT in patients with CTS reveals a recurrent pattern of non-inflammatory fibrosis of the SSCT in the carpal tunnel as a result of repetitive shear stress on the SSCT during finger and wrist movements [5–8]. Over time, this constant mechanical stress leads to the thickening of the SSCT, which impairs the smooth sliding of the MN during tendon loading. As the SSCT swells, it exerts increased pressure within the already narrowed carpal tunnel, subsequently contributing to neuropathic symptoms.

Traditionally, the gold standard for diagnosing CTS has relied on electrophysiologic testing, specifically including nerve conduction studies (NCS) and electromyography (EMG). However, in recent decades, ultrasonography (US) has emerged as a diagnostic tool for CTS. This shift in the diagnostic methodology can be attributed to the inherent advantages of US imaging, including its cost-effectiveness and widespread accessibility [9,10].

Buchberger et al. highlighted key ultrasonographic features in CTS patients, including an increased MN cross-sectional area, increased swelling ratio, and the prominent bowing of the palmar flexor retinaculum [11]. While static US imaging has provided valuable insights, the quest to understand CTS and its effects on MN dynamics has led to the exploration of a dynamic US evaluation in CTS patients. Several studies have reported the dynamic ultrasound evaluation of the MN in CTS patients and suggest that the mobility of MN is reduced in CTS [12–14]. Some investigators have addressed the dynamic assessment of the MN, with particular emphasis on longitudinal MN sliding [15–19] and transverse MN displacement [13,15,17,20–24]. Various methods, such as cross-correlation or speckle tracking algorithms, have been used to study MN dynamics. However, the results of these dynamic MN analyses show some variability, which adds to the complexity of CTS diagnosis and understanding. Longitudinal MN sliding, for example, has yielded inconsistent results across studies. While the results of two studies of longitudinal MN sliding found no significant difference in MN sliding between the CTS group and the control group [15,16], the other three studies reported that CTS patients had less MN sliding than the control group [17–19]. Similarly, the investigation of transverse MN displacement yielded mixed results. Two studies found no statistically significant differences between patients with CTS and the control group [17,20], whereas the other two studies found that MN motion was indeed significantly reduced in the dorsal direction and in the radial direction in CTS patients [21,23]. And another study reported that only the radioulnar axis showed significant differences [25]. In addition, it is worth noting that many of these dynamic analyses were performed by comparing static images or manually tracking the MN, which required considerable time and effort and suffered from poor reproducibility.

In recent years, the field of computer science has witnessed remarkable advances, most notably the development of deep learning (DL) technologies using convolutional neural networks (CNN). DL, with its capability for automatic feature extraction, has found widespread application in medical image processing [26]. In particular, DL has demonstrated remarkable accuracy, sensitivity, and specificity when applied to US images of CTS [27–31]. In particular, Smerilli et al. reported that the mean average precision (mAP), which represents the average of the area under the recall–precision curve, was 0.98, suggesting the high object detection capability of DL [30]. However, despite the promise shown in CTS image analysis, few studies have investigated MN dynamics using DL. The integration of DL models into the study of MN dynamics in CTS patients has the potential to revolutionize the field. In particular, it could lead to a significant reduction in the cost and effort of musculoskeletal dynamics analysis. In this study, we focused on the You Only Look Once (YOLO) model for an object detection AI model. As a one-step detector, YOLO can simultaneously perform object classification and object detection from a single image. Recently, YOLOv5 was released by Glenn Jocher [32], and several studies applying it to breast cancer [33] and bone tumors [34] show good accuracy and precision.

Therefore, the purpose of the present study was to investigate how CTS affects MN dynamics. For this purpose, we used YOLOv5, which is one of the object detection models of DL. To evaluate the kinematics of the MN, we analyzed the transverse displacement and velocity of the MN during the flexion and extension of the finger.

2. Materials and Methods

Seventy hands with no clinical signs of CTS and normal NCS results (control group) and 70 hands affected by CTS who underwent surgery for CTS (CTS group) were included. Out of a total of 140 hands, 100 hands (50 hands in each group) were used to build the machine learning model. The videos of the remaining 40 hands (20 hands in each group) were used to analyze the MN's dynamics. Patients with a history of traumatic injury or wrist surgery to the affected wrist, rheumatoid arthritis, or osteoarthritis of the wrist were excluded. The sample size of MN dynamics analysis was determined based on a careful power analysis using the results of the overall standardized mean difference (SMD) of MN transverse displacement from a pilot study [31] using G*Power 3.1. Preliminary sample

size calculations indicated that a sample of 28 participants (14 in each group) was sufficient to detect differences in MN displacement between the two groups using a *t*-test (effect size = 1.612, $\alpha = 0.01$, power = 0.95).

The diagnosis of CTS was based on a physical examination and NCS. The severity of CTS was graded according to the NCS report [35], resulting in five distinct stages. Stage 1 denotes the normal sensory nerve conduction velocity (SNCV) and distal motor latency (DML). Stage 2 is characterized by a normal SNCV along with a DML greater than 4.5 ms. Stage 3 includes conditions in which the SNCV is less than 40 m/s; the DML exceeds 4.5 ms. Stage 4 is identified by the absence of a sensory response accompanied by a DML greater than 4.5 ms. Finally, stage 5 represents the complete absence of both SNCV and DML responses. The CTS group included only patients classified as stage 2 or higher. Healthy volunteers were included in the control group, along with patients with stage 1 NCS results.

The identification of the MN on short-axis US images was performed just proximal to the carpal tunnel at the wrist crease using an 18 MHz linear probe (Canon APLIO300, Canon Medical Systems, Tochigi, Japan) (Figure 1). The participants actively moved their five fingers from full extension to full flexion (until the fingertips touched the palm) at a metronomic rhythm of 60 cycles per minute in a dorsiflexion neutral position. The recordings, taken at a rate of 30 frames per second, were then cropped to produce a 4 s video. An experienced hand surgeon performed both CTS diagnosis and US imaging.

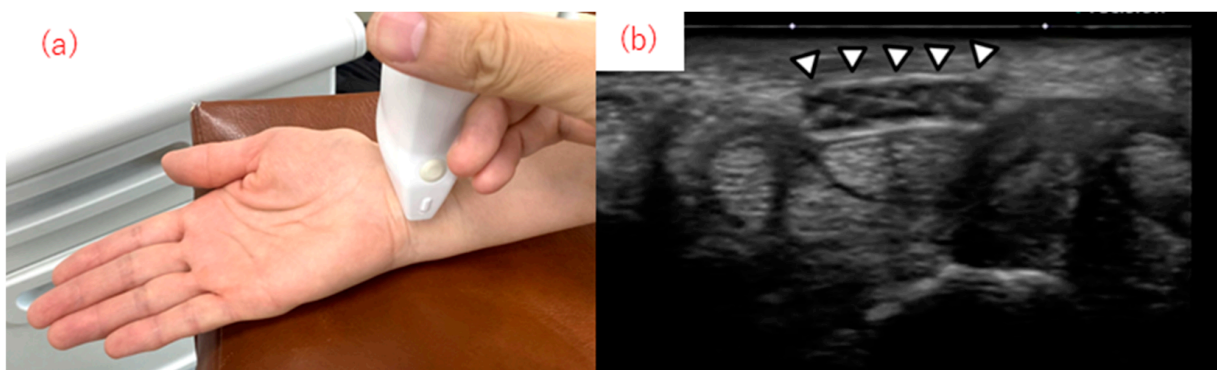


Figure 1. (a) The ultrasound (US) transducer was placed on the palmar side of the wrist crease. Participants actively moved their fingers from full extension to full flexion. (b) US images of the median nerve (white triangles) were obtained using the procedure shown in Figure 1a.

We constructed a model to detect normal MN or CTS using YOLOv5, an object detection algorithm model originally developed by Glenn Jocher [32]. We used 5000 US images containing MN data extracted from 50 hands without CTS and 50 hands with CTS as our basic input data, which were different from the 40 hands used for MN analysis. The amount of data used for training was increased by adding noise to the existing images to compensate for the lack of sample size. This is a common practice in machine learning [36,37]. The CTS detection model was meticulously trained to anticipate and delineate bounding boxes around the MN while simultaneously determining the precise coordinates of the MN (Figure 2). The following software and hardware orchestration was used during the training phase: Ultralytics/YOLOv5, Python-3.7.0, PyTorch-1.7 GPU, and NVIDIA GeForce RTX 3050 laptop GPU. In particular, a stochastic allocation method allocated 80% of the US images to serve as our training dataset, with the remaining 20% reserved for testing purposes. For the object detection task, the YOLOv5 model (parameter size 1.8 M) was used. The hyperparameters were lr0: 0.01, lrf: 0.01, momentum: 0.937, weight_decay: 0.0005, warmup_epochs: 3.0, warmup_momentum: 0.8, warmup_bias_lr: 0.1, box: 0.05, cls: 0.5, cls_pw: 1.0, obj: 1.0, obj_pw: 1.0, anchor_t: 4.0. Transfer learning was performed using the pre-trained weights from YOLOv5 with the US images and the label information of the bounding boxes as the input data. An MN detection task was performed. To evaluate the detection accuracy of the trained models, we examined the mean average precision (mAP),

precision, and recall, all of which are recognized as essential evaluation metrics for object detection models. The term “mAP (0.5)” conveys the mean average precision computed with a threshold of 0.5 within the intersection over the union (IoU) spectrum. Similarly, “mAP (0.5–0.95)” represents the average mAP computed over a range of IoU thresholds of 0.5–0.95 with 0.05 steps.



Figure 2. Images of the CTS detection model showed that it could detect MN by being surrounded by the bounding box.

To begin a detailed analysis of the transverse displacement and velocity of the MN during finger flexion and extension, we obtained the center coordinates of the bounding box (Figure 3a). We then plotted the trajectory of the bounding box to determine the maximum distance of movement in the X coordinate (radial–ulnar direction) and Y coordinate (dorsal–palmar direction), referred to as the X distance and Y distance, respectively (Figure 3b). In addition, we also calculated the average motion velocity in each of the X and Y directions along with the average magnitude velocity, which served as a composite vector. To evaluate the motion velocity, we first calculated the X, Y, and magnitude velocity by determining the motion velocity between successive frames and formulating a composite vector based on the distance traveled between the successive frames. Finally, we analyzed the mean values of these calculated velocities.

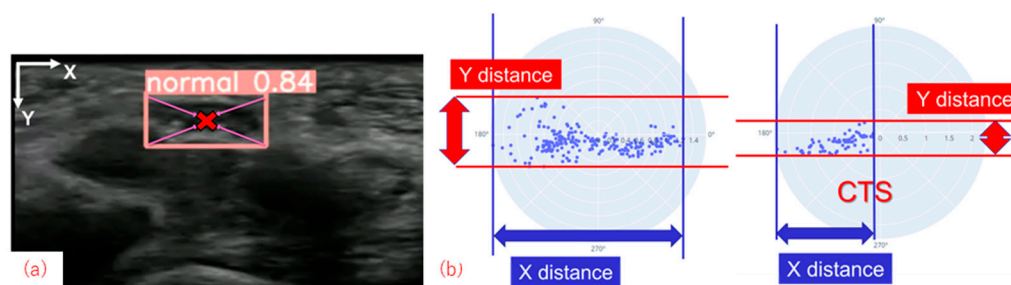


Figure 3. (a) The detection of the center coordinate of the bounding box. The X-axis indicates radial–ulnar direction and the Y-axis indicates dorsal–palmar direction. (b) The trajectory plot. The maximum distance of MN movement was shown as the X distance on the X-axis and as the Y distance on the Y-axis.

All data are presented as the mean \pm standard deviation (SD). The differences between the two groups were statistically tested using a *t*-test, with $p < 0.05$ indicating statistical significance. Statistical analyses were facilitated using an Excel add-in statistical software package (Ekuseru-Toukei 2015, Tokyo, Japan).

3. Results

The detection accuracy of the trained models, which involved a careful comparison between the bounding boxes identified by the trained model and the labeled bounding boxes annotated by expert physicians, was a robust 0.969 for mAP (50) and 0.573 for mAP (50–95). The best score for precision was 0.953, and for recall was 0.956. These analyses were

performed using 20% of our basic input data of 5000 US images derived from 100 hands as test data.

The characteristics of the MN dynamics analysis participants from the remaining 40 hands are shown in Table 1. The control group consisted of twelve males and eight females with a mean age of 55.2 ± 4.52 years, ranging from 32 to 75 years. The CTS group consisted of eight males and twelve females. The mean age was 67.9 ± 2.82 years, ranging from 28 to 80 years. There was no significant age difference between the two groups.

Table 1. The participant’s characteristics.

	Control Group (n = 20)	CTS Group (n = 20)
Age	55.2 (4.52)	67.9 (2.82)
Sex		
Male	12	8
Female	8	12
NCS		
Healthy volunteer	11	-
Stage 1	9	-
Stage 2	-	5
Stage 3	-	7
Stage 4	-	7
Stage 5	-	1

Data were presented as the mean value (standard deviation). Abbreviations: CTS, carpal tunnel syndrome; NCS, nerve conduction study.

The X distance was 3.56 ± 0.39 mm in the control group and 2.04 ± 0.21 mm in the CTS group. The Y distance was 1.06 ± 0.14 mm in the control group and 0.96 ± 0.29 mm in the CTS group (Figure 4). The X distance was significantly shorter in the CTS group than in the control group ($p = 0.0002$), and the Y distance was shorter in the CTS group (not significant). The X distance for each stage of CTS was 2.03 mm (Stage 2), 2.22 mm (Stage 3), 2.08 mm (Stage 4, 5); the Y distance was 1.11 mm (Stage 2), 0.82 mm (Stage 3), 0.80 mm (Stage 4, 5); and there were no significant differences between CTS stage.

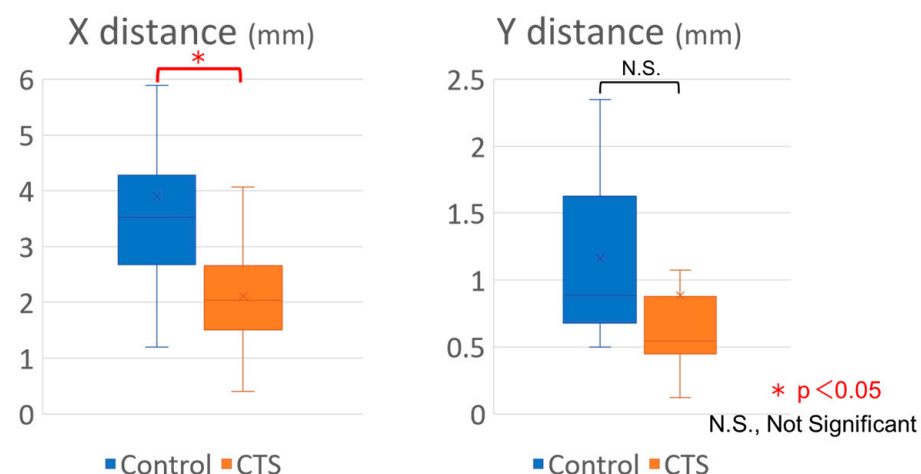


Figure 4. The X distance and Y distance in each group. The X distance in the CTS group was significantly shorter than that of the control group.

When analyzing the MN velocity, the X velocity was 3.74 ± 0.71 mm/s in the control group and 2.71 ± 0.18 mm/s in the CTS group. The Y velocity was 1.39 ± 0.33 mm/s in the control group and 1.02 ± 0.10 mm/s in the CTS group. The magnitude velocity was 4.22 ± 0.81 mm/s in the control group and 3.14 ± 0.22 mm/s in the CTS group. The velocity of Y did not show significant differences between the two groups, and both the

X velocity ($p = 0.03$) and magnitude velocity ($p = 0.03$) showed statistically significant differences (Figure 5). The X velocity for each stage of CTS was 2.46 mm/s (Stage 2), 2.40 mm/s (Stage 3), 2.83 mm/s (Stage 4, 5); the Y velocity was 1.05 mm/s (Stage 2), 0.94 mm/s (Stage 3), 0.96 mm/s (Stage 4, 5); the magnitude velocity was 2.68 mm/s (Stage 2), 2.59 mm/s (Stage 3), 3.01 mm/s (Stage 4, 5); and there were no significant differences between the CTS stages.

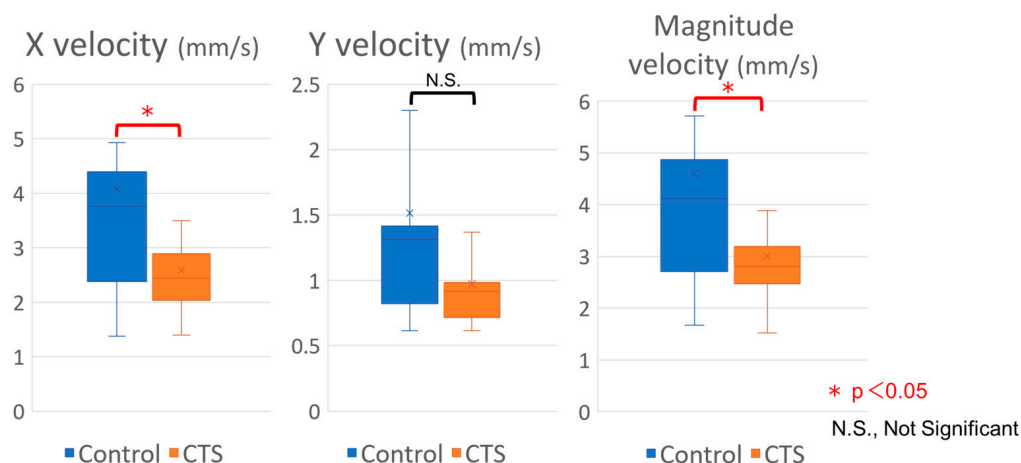


Figure 5. The X velocity and the magnitude velocity were significantly lower in the CTS group than in the control group. The Y velocity showed no significant difference between the two groups.

4. Discussion

In this study, a significant reduction in the radial–ulnar translation distance of the MN during finger movement was observed in patients diagnosed with CTS. This observation is further supported by the notable findings that both radial–ulnar velocity and magnitude velocity were significantly reduced in the CTS group. These findings provide robust support for the hypothesis that fibrosis and adhesions within the SSCT significantly limit the mobility of the MN within the confines of the carpal tunnel, thereby impeding the smooth motion of this important neural structure [3,18]. In particular, this study represents a pioneering effort as it marks the first attempt to meticulously measure both the transverse displacement and velocity of the MN through the use of a state-of-the-art DL model, specifically the CTS detection model. This approach introduces a new dimension to the study of CTS and its impact on MN dynamics.

Typically, the diagnosis of obstructive neuropathies such as CTS has relied primarily on dynamic US imaging, a technique in which the entrapped nerve exhibits atypical spatiotemporal changes due to the motion of adjacent tissues. A meta-analysis dedicated to the evaluation of MN mobility in CTS patients using US imaging revealed interesting findings. In particular, it was shown that CTS patients had consistently reduced MN displacement compared to the healthy controls. The aggregate results of this analysis showed that the standardized mean difference (SMD) was -1.612 (95% confidence interval [CI]: -3.173 to -0.051) during finger flexion or hand grip [31]. Although the reductions in MN displacement in the dorsopalmar and radioulnar axes did not reach statistical significance within the CTS group, the SMD values were -0.795 (95% CI: -1.886 to 0.295) and -0.855 (95% CI: -2.068 to 0.358), respectively [31]. There are 12 previous studies that investigated transverse MN displacement using US imaging, and they showed heterogeneous methodologies. Eight of them compared static images during finger extension and flexion [14,20–23,25,38,39], two used particle tracking via the speckle tracking method [17,40], and one of them introduced a novel algorithm to measure the MN motion area [41]. However, these methods often require the labor-intensive manual tracing of the trapped nerves, and most studies evaluate MN motion only at the initial and final frames, which might not have adequately captured the real-time displacement and dynamics of the MN during finger motion. Only one study used a DL model to quantify the centroid offset of the

MN during finger movement [27]. Various previous studies have reported the transverse MN displacement at the radioulnar axis and the dorsopalmar axis (Tables 2 and 3). In the present study, as in many other studies, MN displacement in the radioulnar axis was significantly lower in the CTS group than in the control group. On the other hand, in the present study, the displacement in the dorsopalmar axis showed no significant difference between the groups in the present study. As described by Nanno et al., the MN is pulled to the radial side by the flexor tendons during finger flexion [22], so the movement on the radioulnar axis might be more susceptible to adhesions with the SSCT and the flexor tendons. In the present study, we successfully assessed not only MN displacement but also MN velocity and demonstrated its reduction in the CTS group, especially in the radioulnar axis. This analysis serves to provide a more nuanced understanding of MN dynamics in the context of CTS and offers the tantalizing prospects of real-time US assessments. Importantly, the results of this study fit seamlessly with previous studies of MN mobility, further validating the robustness of these findings.

Table 2. The results of MN displacement at the radioulnar axis.

	Control Group	CTS Group	<i>p</i> -Value
Yoshii et al. [25]	2.45 (1.76) mm	2.05 (2.82) mm	<0.01
Erel et al. [15]	1.55 (1.04) mm	0.89 (1.15) mm	>0.08
Kang et al. [23]	0.84 (0.18) mm	0.40 (0.13) mm	0.021
The present study	3.56 (0.39) mm	2.04 (0.21) mm	0.0002

Data were expressed as the mean value (standard deviation). Abbreviation: CTS, carpal tunnel syndrome.

Table 3. The results of MN displacement at the dorsopalmer axis.

	Control Group	CTS Group	<i>p</i> -Value
Yoshii et al. [25]	0.377 (0.399) mm	0.069 (0.438) mm	0.06
Kang et al. [23]	0.64 (0.11) mm	0.29 (0.08) mm	0.015
The present study	1.06 (0.14) mm	0.96 (0.29) mm	>0.05

Data were expressed as the mean value (standard deviation). Abbreviation: CTS, carpal tunnel syndrome.

The results of the meta-analysis reported the acceptable precision and accuracy demonstrated by DL models in terms of MN localization and segmentation within the CTS [42]. In an effort to advance the state of knowledge, this study developed a CTS detection model using YOLOv5 as the base model. Using DL object detection models such as U-Net, R-CNN, and their derivatives, several studies have documented the automatic evaluation of the MN within the CTS with US imaging [27–30,43]. While two-step detectors such as R-CNN involve sequential processes, including the identification of candidate regions within an image where objects may reside, followed by classification, one-step detectors such as YOLO offer an alternative paradigm. YOLO directly predicts the bounding box around the target object and its class, allowing for real-time processing capabilities and increased computational efficiency [44]. The effectiveness of these DL models is typically measured by precision and recall, which are widely accepted evaluation metrics that measure the accuracy and robustness of the model. Previous studies have shown commendable results in terms of precision and recall. They showed a precision of 0.890 [41], 0.891 [43], 0.903 [29], 0.960 [30], and a recall of 0.960 [43], 0.912 [45], 0.903 [29], 0.980 [30]. In a previous study using the YOLO model for osteochondritis dissecans (OCD) of the elbow, the YOLOv2 model successfully detected OCD in the object detection task with an average precision of 0.83 [46]. The mAP (50) was 0.998 for the YOLOv5n model and 0.993 for the YOLOv5m model in another study that applied the YOLOv5 to OCD [47]. It is noteworthy that our developed model showed remarkably high values of both precision and recall. Therefore, it can be concluded that YOLO's object detection model performed creditably in the present study, confirming its effectiveness and relevance in the field of CTS diagnosis and evaluation.

Among the reports on the potential of DL in relation to MN, only Wu et al. reported on the morphological characteristics of MN during finger movement. Their investigation yielded an IoU of 0.83 using R-CNN [27], which showed the centroid offset, cross-sectional area, perimeter, and circularity of the MN. In the present study, by assessing MN velocity in addition to displacement during finger movement and comparing this with healthy subjects, we demonstrated that the application of a pre-trained DL model provides a novel way of assessing MN mobility reduction in CTS patients. This study builds on and extends previous studies by demonstrating the possibility of clinical applications of DL models in the diagnosis of CTS through the analysis of US imaging videos.

Several limitations of this study should be acknowledged. First, Nanno et al. reported variations in the MN dynamics, including specifically that the dorsal-palmar deviation of the MN during finger flexion was higher in the wrist positions of dorsal, palmar, radial, and ulnar flexion compared to the neutral position [22]. Although this variance exists, our evaluation was limited to assessing MN dynamics only in the neutral wrist position. This limitation was due to the difficulty of US evaluation in different wrist positions. Therefore, the effect of the wrist position on MN dynamics remains an avenue for future investigation. Second, the sample size of this study, despite careful power analysis using pilot data, was not large. In particular, stage 1 hands without abnormal NCS findings consisted primarily of the contralateral hands of CTS patients and were included in the control group. Although this approach was pragmatic, it may have been necessary to separate this subgroup from the healthy volunteers if the sample size had allowed this. In addition, the limited sample size precluded a detailed examination of the potential correlations between MN mobility and disease severity, which represents another potential avenue for future research.

5. Conclusions

In summary, we conducted a dynamic US analysis of the MN during finger flexion and extension using the YOLOv5 object detection model in the area of DL. The YOLOv5 model demonstrated high accuracy and precision as a CTS detection model. Importantly, our results revealed a significant reduction in the radial–ulnar translation distance and velocity of the MN within the CTS group, providing robust evidence of the limitations imposed by fibrosis and adhesions within SSCT. This study, the first of its kind to quantify both transverse displacement and the velocity of the MN using DL's CTS detection model, opens new avenues for research and clinical applications in the field of CTS diagnosis and treatment.

Author Contributions: Conceptualization, S.T. (Shuya Tanaka) and A.I.; methodology, A.I.; software, A.I., H.N. and I.S.; validation, S.T. (Shuya Tanaka), I.S., T.F., T.K. and M.K.; formal analysis, S.T. (Shuya Tanaka); investigation, S.T. (Shuya Tanaka) and I.S.; resources, A.I., I.S., Y.E. and S.T. (Shunsaku Takigami); data curation, S.T. (Shuya Tanaka); writing—original draft preparation, S.T. (Shuya Tanaka); writing—review and editing, A.I. and Y.M.; visualization, S.T. (Shuya Tanaka); supervision, A.I.; project administration, R.K. All authors have read and agreed to the published version of the manuscript.

Funding: This research received no external funding.

Institutional Review Board Statement: This study was conducted in accordance with the Declaration of Helsinki and approved by the Ethics Committee of Kobe University Graduate School of Medicine (No. B21009; 21 April 2021).

Informed Consent Statement: Informed consent was obtained from all subjects involved in this study.

Data Availability Statement: The data presented in this study are available upon request from the corresponding author. The data are not publicly available because of confidentiality concerns.

Conflicts of Interest: The authors declare no conflict of interest.

References

1. Alfonso, C.; Jann, S.; Massa, R.; Torreggiani, A. Diagnosis treatment and follow-up of the carpal tunnel syndrome: A review. *Neurol. Sci.* **2010**, *31*, 243–252. [[CrossRef](#)] [[PubMed](#)]
2. Atroshi, I.; Gummesson, C.; Johnsson, R.; Ornstein, E.; Ranstam, J.; Rosen, I. Prevalence of carpal tunnel syndrome in a general population. *JAMA* **1999**, *282*, 153–158. [[CrossRef](#)] [[PubMed](#)]
3. Festen-Schrier, V.J.M.M.; Amadio, P.C. The biomechanics of subsynovial connective tissue in health and its role in carpal tunnel syndrome. *J. Electromyogr. Kinesiol.* **2018**, *38*, 232–239. [[CrossRef](#)]
4. Robben, E.; Dever, J.; De Groef, A.; Degreef, I.; Peers, K. Subsynovial connective tissue thickness in carpal tunnel syndrome: A systematic review. *Clin. Biomech.* **2020**, *75*, 105002. [[CrossRef](#)] [[PubMed](#)]
5. Ettema, A.M.; Amadio, P.C.; Zhao, C.; Wold, L.E.; O’Byrne, M.M.; Moran, S.L.; An, K.N. Changes in the functional structure of the tenosynovium in idiopathic carpal tunnel syndrome: A scanning electron microscope study. *Plast. Reconstr. Surg.* **2006**, *118*, 1413–1422. [[CrossRef](#)] [[PubMed](#)]
6. Ettema, A.M.; Amadio, P.C.; Zhao, C.; Wold, L.E.; An, K.N. A histological and immunohistochemical study of the subsynovial connective tissue in idiopathic carpal tunnel syndrome. *J. Bone Jt. Surg. Am.* **2004**, *86*, 1458–1466. [[CrossRef](#)]
7. Kerr, C.D.; Sybert, D.R.; Albarracin, N.S. An analysis of the flexor synovium in idiopathic carpal tunnel syndrome: Report of 625 cases. *J. Hand Surg. Am.* **1992**, *17*, 1028–1030. [[CrossRef](#)] [[PubMed](#)]
8. Oh, J.; Zhao, C.; Zobitz, M.E.; Wold, L.E.; An, K.N.; Amadio, P.C. Morphological changes of collagen fibrils in the subsynovial connective tissue in carpal tunnel syndrome. *J. Bone Jt. Surg. Am.* **2006**, *88*, 824–831. [[CrossRef](#)]
9. Chen, Y.T.; Williams, L.; Zak, M.J.; Fredericson, M. Review of Ultrasonography in the Diagnosis of Carpal Tunnel Syndrome and a Proposed Scanning Protocol. *J. Ultrasound Med.* **2016**, *35*, 2311–2324. [[CrossRef](#)]
10. Visser, L.H.; Smidt, M.H.; Lee, M.L. High-resolution sonography versus EMG in the diagnosis of carpal tunnel syndrome. *J. Neurol. Neurosurg. Psychiatry* **2008**, *79*, 63–67. [[CrossRef](#)]
11. Buchberger, W.; Judmaier, W.; Birbamer, G.; Lener, M.; Schmidauer, C. Carpal tunnel syndrome: Diagnosis with high-resolution sonography. *Am. J. Roentgenol.* **1992**, *159*, 793–798. [[CrossRef](#)] [[PubMed](#)]
12. Kluge, S.; Langer, M.; Schelle, T. Sonographic Diagnosis of Carpal Tunnel Syndrome. *Hand Clin.* **2022**, *38*, 35–53. [[CrossRef](#)] [[PubMed](#)]
13. Ellis, R.; Blyth, R.; Arnold, N.; Miner-Williams, W. Is there a relationship between impaired median nerve excursion and carpal tunnel syndrome? A systematic review. *J. Hand Ther.* **2017**, *30*, 3–12. [[CrossRef](#)] [[PubMed](#)]
14. Park, G.Y.; Kwon, D.R.; Seok, J.I.; Park, D.S.; Cho, H.K. Usefulness of ultrasound assessment of median nerve mobility in carpal tunnel syndrome. *Acta Radiol.* **2018**, *59*, 1494–1499. [[CrossRef](#)] [[PubMed](#)]
15. Erel, E.; Dilley, A.; Greening, J.; Morris, V.; Cohen, B.; Lynn, B. Longitudinal sliding of the median nerve in patients with carpal tunnel syndrome. *J. Hand Surg. Br.* **2003**, *28*, 439–443. [[CrossRef](#)] [[PubMed](#)]
16. Hough, A.D.; Moore, A.P.; Jones, M.P. Reduced longitudinal excursion of the median nerve in carpal tunnel syndrome. *Arch. Phys. Med. Rehabil.* **2007**, *88*, 569–576. [[CrossRef](#)] [[PubMed](#)]
17. Filius, A.; Scheltens, M.; Bosch, H.G.; van Doorn, P.A.; Stam, H.J.; Hovius, S.E.; Amadio, P.C.; Selles, R.W. Multidimensional ultrasound imaging of the wrist: Changes of shape and displacement of the median nerve and tendons in carpal tunnel syndrome. *J. Orthop. Res.* **2015**, *33*, 1332–1340. [[CrossRef](#)]
18. Filius, A.; Thoreson, A.R.; Wang, Y.; Passe, S.M.; Zhao, C.; An, K.N.; Amadio, P.C. The effect of tendon excursion velocity on longitudinal median nerve displacement: Differences between carpal tunnel syndrome patients and controls. *J. Orthop. Res.* **2015**, *33*, 483–487. [[CrossRef](#)]
19. Liu, C.T.; Liu, D.H.; Chen, C.J.; Wang, Y.W.; Wu, P.S.; Horng, Y.S. Effects of wrist extension on median nerve and flexor tendon excursions in patients with carpal tunnel syndrome: A case control study. *BMC Musculoskelet. Disord.* **2021**, *22*, 477. [[CrossRef](#)]
20. Wang, Y.; Filius, A.; Zhao, C.; Passe, S.M.; Thoreson, A.R.; An, K.N.; Amadio, P.C. Altered median nerve deformation and transverse displacement during wrist movement in patients with carpal tunnel syndrome. *Acad. Radiol.* **2014**, *21*, 472–480. [[CrossRef](#)]
21. Van Doesburg, M.H.; Henderson, J.; van der Molen, A.B.M.; An, K.N.; Amadio, P.C. Transverse plane tendon and median nerve motion in the carpal tunnel: Ultrasound comparison of carpal tunnel syndrome patients and healthy volunteers. *PLoS ONE* **2012**, *7*, e37081. [[CrossRef](#)] [[PubMed](#)]
22. Nanno, M.; Sawaizumi, T.; Kodera, N.; Tomori, Y.; Takai, S. Transverse Movement of the Median Nerve in the Carpal Tunnel during Wrist and Finger Motion in Patients with Carpal Tunnel Syndrome. *Tohoku J. Exp. Med.* **2015**, *236*, 233–240. [[CrossRef](#)] [[PubMed](#)]
23. Kang, H.J.; Yoon, J.S. Effect of finger motion on transverse median nerve movement in the carpal tunnel. *Muscle Nerve* **2016**, *54*, 738–742. [[CrossRef](#)] [[PubMed](#)]
24. Toge, Y.; Nishimura, Y.; Basford, J.R.; Nogawa, T.; Yamanaka, M.; Nakamura, T.; Yoshida, M.; Nagano, A.; Tajima, F. Comparison of the effects of flexion and extension of the thumb and fingers on the position and cross-sectional area of the median nerve. *PLoS ONE* **2013**, *8*, e83565. [[CrossRef](#)] [[PubMed](#)]
25. Yoshii, Y.; Ishii, T.; Tung, W.-L.; Sakai, S.; Amadio, P.C. Median nerve deformation and displacement in the carpal tunnel during finger motion. *J. Orthop. Res.* **2013**, *31*, 1876–1880. [[CrossRef](#)] [[PubMed](#)]
26. Lalehzarian, S.P.; Gowd, A.K.; Liu, J.N. Machine learning in orthopaedic surgery. *World J. Orthop.* **2021**, *12*, 685–699. [[CrossRef](#)]

27. Wu, C.H.; Syu, W.T.; Lin, M.T.; Yeh, C.L.; Boudier-Revéret, M.; Hsiao, M.Y.; Kuo, P.L. Automated Segmentation of Median Nerve in Dynamic Sonography Using Deep Learning: Evaluation of Model Performance. *Diagnostics* **2021**, *11*, 1893. [CrossRef]
28. Wang, Y.W.; Chang, R.F.; Horng, Y.S.; Chen, C.J. MNT-DeepSL: Median nerve tracking from carpal tunnel ultrasound images with deep similarity learning and analysis on continuous wrist motions. *Comput. Med. Imaging Graph.* **2020**, *80*, 101687. [CrossRef]
29. Cosmo, M.D.; Chiara Fiorentino, M.; Villani, F.P.; Sartini, G.; Smerilli, G.; Filippucci, E.; Frontoni, E.; Moccia, S. Learning-based median nerve segmentation from ultrasound images for carpal tunnel syndrome evaluation. In Proceedings of the 2021 43rd Annual International Conference of the IEEE Engineering in Medicine & Biology Society (EMBC), Virtual Conference, 1–5 November 2021; pp. 3025–3028.
30. Smerilli, G.; Cipolletta, E.; Sartini, G.; Moscioni, E.; Di Cosmo, M.; Fiorentino, M.C.; Moccia, S.; Frontoni, E.; Grassi, W.; Filippucci, E. Development of a convolutional neural network for the identification and the measurement of the median nerve on ultrasound images acquired at carpal tunnel level. *Arthritis Res. Ther.* **2022**, *24*, 38. [CrossRef]
31. Huang, Y.T.; Chen, C.J.; Wang, Y.W.; Peng, P.L.; Luo, Y.T.; Horng, Y.S. Ultrasonographical Evaluation of the Median Nerve Mobility in Carpal Tunnel Syndrome: A Systematic Review and Meta-Analysis. *Diagnostics* **2022**, *12*, 2349. [CrossRef]
32. YOLOv5 in PyTorch > ONNX > CoreML > TFLite—GitHub. Available online: <https://github.com/ultralytics/yolov5> (accessed on 17 January 2022).
33. Aly, G.H.; Marey, M.; El-Sayed, S.A.; Tolba, M.F. YOLO Based Breast Masses Detection and Classification in Full-Field Digital Mammograms. *Comput. Methods Programs Biomed.* **2021**, *200*, 105823. [CrossRef]
34. Li, J.; Li, S.; Li, X.; Miao, S.; Dong, C.; Gao, C.; Liu, X.; Hao, D.; Xu, W.; Huang, M.; et al. Primary bone tumor detection and classification in full-field bone radiographs via YOLO deep learning model. *Eur. Radiol.* **2023**, *33*, 4237–4248. [CrossRef] [PubMed]
35. Shinohara, I.; Inui, A.; Mifune, Y.; Nishimoto, H.; Yamaura, K.; Mukohara, S.; Yoshikawa, T.; Kato, T.; Furukawa, T.; Hoshino, Y.; et al. Using deep learning for ultrasound images to diagnose carpal tunnel syndrome with high accuracy. *Ultrasound Med. Biol.* **2022**, *48*, 2052–2059. [CrossRef]
36. Amodeo, I.; De Nunzio, G.; Raffaeli, G.; Borzani, I.; Griggio, A.; Conte, L.; Macchini, F.; Condò, V.; Persico, N.; Fabietti, I.; et al. A machine and deep Learning Approach to predict pulmonary hypertension in newborns with congenital diaphragmatic hernia (CLANNISH): Protocol for a retrospective study. *PLoS ONE* **2021**, *16*, e0259724. [CrossRef] [PubMed]
37. Taormina, V.; Raso, G.; Gentile, V.; Abbene, L.; Buttacavoli, A.; Bonsignore, G.; Valenti, C.; Messina, P.; Scardina, G.A.; Cascio, D. Automated Stabilization, Enhancement and Capillaries Segmentation in Videocapillaroscopy. *Sensors* **2023**, *23*, 7674. [CrossRef]
38. Nakamichi, K.; Tachibana, S. Restricted Motion of the Median Nerve in Carpal Tunnel Syndrome. *J. Hand Surg.* **1995**, *20*, 460–464. [CrossRef] [PubMed]
39. Fan, C.; Fede, C.; Pirri, C.; Guidolin, D.; Biz, C.; Macchi, V.; De Caro, R.; Stecco, C. Quantitative Evaluation of the Echo Intensity of Paraneural Area and Myofascial Structure around Median Nerve in Carpal Tunnel Syndrome. *Diagnostics* **2020**, *10*, 914. [CrossRef] [PubMed]
40. Kuo, T.-T.; Lee, M.-R.; Liao, Y.-Y.; Chen, J.-P.; Hsu, Y.-W.; Yeh, C.-K. Assessment of Median Nerve Mobility by Ultrasound Dynamic Imaging for Diagnosing Carpal Tunnel Syndrome. *PLoS ONE* **2016**, *11*, e0147051. [CrossRef]
41. Hara, Y.; Tajiri, Y.; Kawano, K.; Hoshikawa, S. Evaluation of Restricted Motion Area of the Median Nerve in Patients with Carpal Tunnel Syndrome: A New Measurement Method Using an Ultrasonographic Video Image. *J. Hand Surg.* **2021**, *26*, 635–643. [CrossRef]
42. Wang, J.C.; Shu, Y.C.; Lin, C.Y.; Wu, W.T.; Chen, L.R.; Lo, Y.C.; Chiu, H.C.; Özçakar, L.; Chang, K.V. Application of deep learning algorithms in automatic sonographic localization and segmentation of the median nerve: A systematic review and meta-analysis. *Artif. Intell. Med.* **2023**, *137*, 102496. [CrossRef]
43. Hafiane, A.; Vieyres, P.; Delbos, A. Deep Learning with Spatiotemporal Consistency for Nerve Segmentation in Ultrasound Images. *arXiv* **2017**, arXiv:1706.05870.
44. Redmon, J.; Divvala, S.; Girshick, R.; Farhadi, A. You only look once: Unified, real-time object detection. In Proceedings of the IEEE Conference on Computer Vision and Pattern Recognition, Las Vegas, NV, USA, 27–30 June 2016.
45. Horng, M.H.; Yang, C.W.; Sun, Y.N.; Yang, T.H. DeepNerve: A New Convolutional Neural Network for the Localization and Segmentation of the Median Nerve in Ultrasound Image Sequences. *Ultrasound Med. Biol.* **2020**, *46*, 2439–2452. [CrossRef] [PubMed]
46. Shinohara, I.; Yoshikawa, T.; Inui, A.; Mifune, Y.; Nishimoto, H.; Mukohara, S.; Kato, T.; Furukawa, T.; Tanaka, S.; Kusunose, M.; et al. Degree of Accuracy with Which Deep Learning for Ultrasound Images Identifies Osteochondritis Dissecans of the Humeral Capitellum. *Am. J. Sports Med.* **2023**, *51*, 358–366. [CrossRef] [PubMed]
47. Inui, A.; Mifune, Y.; Nishimoto, H.; Mukohara, S.; Fukuda, S.; Kato, T.; Furukawa, T.; Tanaka, S.; Kusunose, M.; Takigami, S.; et al. Detection of Elbow OCD in the Ultrasound Image by Artificial Intelligence Using YOLOv8. *Appl. Sci.* **2023**, *13*, 7623. [CrossRef]

Disclaimer/Publisher’s Note: The statements, opinions and data contained in all publications are solely those of the individual author(s) and contributor(s) and not of MDPI and/or the editor(s). MDPI and/or the editor(s) disclaim responsibility for any injury to people or property resulting from any ideas, methods, instructions or products referred to in the content.